Dynamics of a Multicomponent Dark Energy Model and the Possibility of Early Dark Energy Like Behaviour

Prasanta Sahoo,[1, *] Nandan Roy,[2, †] and Himadri Shekhar Mondal[1, ‡]

[1]*Midnapore College (Autonomous), Midnapore, West Bengal, India, 721101*
[2]*NAS, Centre for Theoretical Physics & Natural Philosophy, Mahidol University,*
Nakhonsawan Campus, Phayuha Khiri, Nakhonsawan 60130, Thailand

This study explores the dynamics and phase-space behavior of a multicomponent dark energy model, where the dark sector consists of a minimally coupled canonical scalar field and the cosmological constant, using a dynamical system analysis setup for various types of potentials for which a general parameterisation of the scalar field potentials has been considered. Several fixed points with different cosmological behaviours have been identified. A detailed stability analysis has been done and possible late-time attractors have been found. For this multi-component dark energy model, the late-time attractors are either fully dominated by the cosmological constant or represent a scenario where a combination of the scalar field and the cosmological constant dominates the universe. We have also shown that for this type of model, the scalar field can show early dark energy (EDE) like behaviour. However, our analysis indicates that this EDE like behaviour occurs naturally deep in the matter-dominated era, not before the recombination era.

I. INTRODUCTION

Over two decades, various cosmological observations have confirmed the ongoing accelerated expansion of the universe [1–5], yet the cause of it remains unknown. In the standard model of cosmology, we consider the accelerated expansion to be driven by the cosmological constant [6], which is consistent with current cosmological observations. However, it faces several challenges from both theoretical and observational perspectives, despite its significant achievements.

In addition to theoretical issues such as the cosmological constant problem and the fine-tuning problem, recent precision cosmological data have revealed a significant statistical discrepancy in the estimation of the Hubble parameter (H_0) between early-time and late-time observations. This discrepancy presents an additional challenge to the cosmological constant. Early universe measurements (e.g., CMB Planck [7], BAO [8, 9], BBN [10], DES [11–13]) estimate $H_0 \approx (67.0 - 68.5)$ km/s/Mpc. In contrast, late-time measurements (e.g. SH0ES [14] and H0LiCOW [15]) using time-delay cosmography find $H_0 = (74.03 \pm 1.42)$ km/s/Mpc. This $\simeq 5.3\sigma$ discrepancy [16] hints towards new physics beyond ΛCDM in the dark energy sector.

Various dynamical dark-energy models have been suggested as alternatives for the cosmological constant [17, 18]. For dynamical dark energy models the equation of state of the dark energy changes over time [19–27]. These models include but are not limited to quintessence, k-essence, and phantom-type scalar field models, where generally a scalar field is coupled with the matter minimally or non-minimally with a associated potential which can generate sufficient negative pressure to drive the accelerated expansion of the universe. Recent observations from DESI collaboration [28, 29] and other literatures [30–33] have pointed towards the evidence for the dynamical nature of the dark energy over the cosmological constant.

Recent literature also shows evidence towards the possibility of a multi-component nature of the dark energy sector. These models are more preferable compared to the cosmological constant when aligned with current observations [27, 34–37]. In these types of models, the dark sector is considered to consist of cosmological constant together with other dark energy components like a scalar field[34] or a fluid[35], or to be composed of multi-scalar fields[27]. In addition, these models can significantly reduce Hubble tension compared to the ΛCDM model[27, 34].

In this paper, we have investigated a multicomponent dark energy model where the dark sector comprises a minimally coupled canonical scalar field, known as a quintessence field, and a cosmological constant. Our primary goal is to examine the phase space behaviour and dynamics of this composite model using the dynamical systems approach. By applying appropriate variable transformations, we convert the system of equations into a set of autonomous equations. Subsequently, these equations are recast in polar form to facilitate mathematical handling. We have considered a parameterization of the scalar field potential that can encompass various forms of potential to keep our analysis as general as possible, as there is no consensus on the choice for the form of the scalar field potential. A detailed stability analysis

of the system is presented. Additionally, we explore the dynamics of this model by numerically solving it, revealing some naturally occurring Early Dark Energy (EDE) like behaviours of the scalar field.

The manuscript is structured as follows. In Section II, we cover the mathematical setup of the model. Section III forms the autonomous system, which is then transformed into polar form in Section IV. Section V provides a detailed stability analysis of the system. In Section VI, we explore the EDE like behaviour of the scalar field with various potentials. Finally, in Section VII, we summarise and conclude our findings.

II. MATHEMATICAL BACKGROUND

In a spatially flat universe described by the standard FLRW metric which includes relativistic components, matter components, a minimally coupled canonical scalar field known as the quintessence field, and the cosmological constant; the Friedmann equations can be expressed as follows:

$$H^2 = \frac{\kappa^2}{3} \left(\rho_m + \rho_r + \rho_\phi + \rho_\Lambda \right), \tag{1}$$

$$\dot{H} = -\frac{\kappa^2}{2} \sum_i \left(p_i + \rho_i \right). \tag{2}$$

Here, $\kappa^2 = 8\pi G$, with $H = \dot{a}/a$ denoting the Hubble parameter and $a(t)$ representing the scale factor. The terms $p_\phi = \frac{1}{2}\dot{\phi}^2 + V(\phi)$ and $\rho_\phi = \frac{1}{2}\dot{\phi}^2 - V(\phi)$ correspond to the pressure and energy density of the scalar field. The subscripts m, r, ϕ, and Λ refer to matter, radiation, quintessence, and the cosmological constant, respectively. The pressure p_i and the energy density ρ_i for each species i, namely m, r, ϕ, and Λ, are interrelated through the relation $p_i = w_i \rho_i$, where

$$w_i = \begin{cases} \frac{1}{3}, & \text{for relativistic matter} \\ 0, & \text{for non-relativistic matter} \\ -1, & \text{for } \Lambda. \end{cases}$$

The Klein-Gordon equation for the scalar field and the continuity equations, respectively, can be expressed as follows:

$$\ddot{\phi} + 3H\dot{\phi} + \frac{dV(\phi)}{d\phi} = 0, \tag{3}$$

$$\dot{\rho}_i = -3H(p_i + \rho_i), \quad \forall \quad i = m, r, \phi, \Lambda. \tag{4}$$

The density parameter for a given species 'i' is expressed as $\Omega_i = \frac{k^2 \rho_i}{3H^2}$. Consequently, the Friedmann constraint can be written as,

$$\Omega_m + \Omega_r + \Omega_\phi + \Omega_\Lambda = 1. \tag{5}$$

III. THE DYNAMICAL SYSTEM

To understand the phase-space behavior of the system, one needs to introduce a new set of dimensionless variables to write it as an autonomous system. Here we consider the following set of dimensionless transformations:

$$x^2 = \frac{\kappa^2 \dot{\phi}^2}{6H^2}, \quad y^2 = \frac{\kappa^2 V(\phi)}{3H^2}, \tag{6}$$

$$\lambda = -\frac{1}{kV}\frac{dV(\phi)}{d\phi}, \Gamma = \frac{V\frac{d^2V}{d\phi^2}}{\left(\frac{dV}{d\phi}\right)^2}.$$

With the help of the above transformations, the system can be reduced to a set of autonomous equations;

$$x' = -3x + \sqrt{\frac{3}{2}}\lambda y^2 + \frac{1}{2}x\left(6x^2 + 3\Omega_m + 4\Omega_r\right), \tag{7a}$$

$$y' = -\sqrt{\frac{3}{2}}\lambda xy + \frac{1}{2}y\left(6x^2 + 3\Omega_m + 4\Omega_r\right), \tag{7b}$$

$$\Omega'_m = \Omega_m\left(-3 + 6x^2 + 3\Omega_m + 4\Omega_r\right), \tag{7c}$$

$$\Omega'_r = \Omega_r\left(-4 + 6x^2 + 3\Omega_m + 4\Omega_r\right), \tag{7d}$$

$$\lambda' = -\sqrt{6}x(\Gamma - 1)\lambda^2 = -\sqrt{6}xf. \tag{7e}$$

Here, the derivatives are with respect to $N = ln\left(\frac{a}{a_0}\right)$ and $f = (\Gamma - 1)\lambda^2$, where a_0 is the present value of the scale factor. In such a scenario, the total Equation of State (EoS) can be written as

$$\omega_{tot} \equiv \frac{p_{tot}}{\rho_{tot}} = -1 + 2x^2 + \Omega_m + \frac{4}{3}\Omega_r. \tag{8}$$

The system of equations given in Eq.(7) cannot be a closed system due to the arbitrariness of the form of the scalar field potential $V(\phi)$. To close the system, one needs to find f as a function of variables x, y, λ. Since by definition f contains the derivative of the potential, the form of it will depend only on the choice of the potential.

Thus, for a particular choice of potential, there will be a corresponding form of f. It is also possible to consider a particular form of the f and find the corresponding potential using the definition of

the y, λ and Γ variable given in Eq.(6). In this work, we consider $f = \alpha_0 + \alpha_1 \lambda + \alpha_2 \lambda^2$, where the parameters α_0, α_1 and α_2 can take any real value. This particular parametrisation of f was first proposed in [38]. Different choices of the α_0, α_1 and α_2 parameters will correspond to different classes of potentials. In Table-I, we list eight distinct classes of potentials, each corresponding to different choices of the α parameters. The classification was made based on whether certain α parameters are zero or not. This approach has been taken to facilitate our analysis for a wide class of potentials in a single setup. A similar approach but for a different choice of dynamical variables has also been used in [39].

IV. REPRESENTATION OF THE DYNAMICAL SYSTEM IN POLAR FORM

The use of polar coordinates to study the cosmological system is often useful, as shown in [38–40] because the new variables are directly related to the cosmological parameters and the mathematical handling of the system becomes easier. To transform the system of equations Eq.(7) into polar form, we use the transformation $x = r \cos\theta$ and $y = r \sin\theta$, where $r^2 = x^2 + y^2 = \Omega_\phi$. With the above choice, the system of equations reduces to

$$r' = \frac{r}{2}\left(-3 - 3\cos(2\theta) + 6r^2\cos^2\theta + 3\Omega_m + 4\Omega_r\right),$$
(9a)

$$\theta' = \frac{1}{2}\sin\theta\left(6\cos\theta - \sqrt{6}\lambda r\right),$$
(9b)

$$\Omega_m' = \Omega_m\left(-3 + 6r^2\cos^2\theta + 3\Omega_m + 4\Omega_r\right),$$
(9c)

$$\Omega_r' = \Omega_r\left(-4 + 6r^2\cos^2\theta + 3\Omega_m + 4\Omega_r\right),$$
(9d)

$$\lambda' = -\sqrt{6}r\cos\theta\left(\alpha_0 + \alpha_1\lambda + \alpha_2\lambda^2\right).$$
(9e)

In addition, the Friedmann constraint given in Eq.(5) takes the following form

$$r^2 + \Omega_m + \Omega_r + \Omega_\Lambda = 1.$$
(10)

The total equation of state and the equation of state of the scalar field can be represented in the polar form as follows,

$$\omega_{tot} = -1 + 2r^2\cos^2\theta + \Omega_m + \frac{4}{3}\Omega_r,$$
(11)

$$\omega_\phi \equiv \frac{p_\phi}{\rho_\phi} = \cos 2\theta.$$
(12)

V. STABILITY ANALYSIS

The equilibrium points of the system of equations given in Eq.(9) are listed in Table-II, while the eigenvalues corresponding to these points are presented in Table-III. The equilibrium points are calculated by solving the simultaneous system of equations: $r' = 0$, $\theta' = 0$, $\Omega_m' = 0$, $\Omega_r' = 0$, and $\lambda' = 0$. The existence of equilibrium points for the corresponding potentials is also given in the last column of the Table-II. The values for the cosmological parameters, such as the deceleration parameter, the equation of state (EoS) of the scalar field, and the total EoS for each fixed point, are provided in Table-IV.

In this context, the subscript 'c' is used to denote the equilibrium points (r_c, θ_c, Ω_{mc}, Ω_{rc}, λ_c). Subsequently, we analyze the stability of these equilibrium points by categorizing them according to the different epochs of the universe they represent.

A. Radiation Dominated Era

The equilibrium points indicating the radiation domination era are characterised by $\Omega_{rc} = 1$ and represented by 'r' which are of the nonisolated type and given in Table-II. For all the equilibrium points of this era, the corresponding Jacobian matrix has two different sets of eigenvalues depending on whether $\theta_c = n\pi$ or $\theta_c = n\pi \pm \frac{\pi}{2}$. Those eigenvalues are listed in Table-III. In both cases, the Jacobian matrix has both positive and negative eigenvalues. So, these equilibrium points are saddle-like in nature. These equilibrium points exist for all potentials ($V_1 - V_8$) listed in Table-I. From Table-IV it can be seen as expected that at these equilibrium points the universe is decelerating, and $w_{tot} = 1/3$.

B. Matter Dominated Era

The equilibrium points indicating the matter dominated era are defined by $\Omega_{mc} = 1$, are denoted by 'm' and given in the Table-II. The Jacobian matrix, corresponding to any equilibrium point during this era, exhibits two distinct sets of eigenvalues depending on whether $\theta_c = n\pi$ or $\theta_c = n\pi \pm \frac{\pi}{2}$. These eigenvalues are detailed in Table-III. For each $n \in \mathbb{Z}$, the equilibrium points during this period are categorized as saddle points due to the presence of both positive and negative eigenvalues corresponding to these fixed points. The equilibrium points for the matter domination era are present for all potentials $V_1 - V_8$. One can see from Table-IV that these points represent a decelerating universe with $w_{tot} = 0$.

Label	Structure of f	Potential $V(\phi)$
V_1	$\alpha_0 \neq 0,\ \alpha_1 \neq 0,\ \alpha_2 \neq 0$	$A\,exp\left[\dfrac{\alpha_1 k\phi - 2\log\left(\cosh\left(\frac{1}{2}\sqrt{\alpha_1^2 - 4\alpha_0\alpha_2}\,k(\phi+B)\right)\right)}{2\alpha_2}\right]$
V_2	$\alpha_0 = 0,\ \alpha_1 \neq 0,\ \alpha_2 \neq 0$	$A\left(e^{\alpha_1 k\phi}\right)^{\frac{1}{\alpha_2}}\left(\alpha_1\alpha_2 k\left(e^{\alpha_1 k\phi} + \alpha_2 e^{\alpha_1 Ak}\right)\right)^{-\frac{1}{\alpha_2}}$
V_3	$\alpha_0 \neq 0,\ \alpha_1 = 0,\ \alpha_2 \neq 0$	$A\cos^{-\frac{1}{\alpha_2}}\left(\sqrt{\alpha_0\alpha_2}\,k(\phi+B)\right)$
V_4	$\alpha_0 \neq 0,\ \alpha_1 \neq 0,\ \alpha_2 = 0$	$A\,exp\left[\dfrac{\alpha_0 k^2\phi - c_1 e^{-k\alpha_1\phi}}{\alpha_1 k}\right]$
V_5	$\alpha_0 \neq 0,\ \alpha_1 = 0,\ \alpha_2 = 0$	$A\,exp\left[\frac{1}{2}\alpha_0 k^2\phi^2 + B\phi\right]$
V_6	$\alpha_0 = 0,\ \alpha_1 \neq 0,\ \alpha_2 = 0$	$A\,exp\left[-\dfrac{Be^{-k\alpha_1\phi}}{\alpha_1 k}\right]$
V_7	$\alpha_0 = 0,\ \alpha_1 = 0,\ \alpha_2 \neq 0$	$A\left(\alpha_2\phi + B\right)^{-\frac{1}{\alpha_2}}$
V_8	$\alpha_0 = 0,\ \alpha_1 = 0,\ \alpha_2 = 0$	$Ae^{B\phi}$

TABLE I: A list of various classes of potentials based on the different choices for the α parameters. Here A and B are integration constants.

C. Scalar field dominated era

For the equilibrium points in the scalar field domination era, we have $r_c = 1$. In this case, the equilibrium points are given by $e1$ - $e4_{\pm}$ in Table-II. The eigenvalues of the Jacobian matrix at $e1$ depend on α_1. But, for the existence of positive eigenvalues of the Jacobian matrix at $e1$, the equilibrium points given by $e1$ are unstable and exist for the potentials V_2 and $V_6 - V_8$. These equilibrium points represent a decelerating universe with $w_{tot} = 1$.

The equilibrium points indicated by $e2$ are of non-hyperbolic nature, characterised by a zero eigenvalue. These fixed points may be stable within the parameter range $0 < \alpha_0 \leq \frac{3}{4}$, as the remaining two eigenvalues can be negative. Due to their non-hyperbolic nature, linear stability analysis cannot determine their stability. Instead, stability must be assessed using centre manifold theory or by numerically plotting the system's phase around the fixed point. Given that the system's dimension exceeds three, a complete phase plot is impractical; hence, phase portraits are drawn on various projected planes. If all projected phase planes depict the equilibrium point as stable, it is stable in the full space. Conversely, if any projected phase space shows instability, the equilibrium point is unstable in the entire space. For the equilibrium point $e2$, we draw a phase plot (Fig.1) in the (r, Ω_m) plane. This phase plot indicates that the equilibrium points specified by $e2$ are unstable on the (r, Ω_m) plane and consequently in the full space. Those equilibrium points represent an accelerating universe with $w_{\phi} = w_{tot} = -1$.

The equilibrium points, labelled $e3$ and $e4_{\pm}$, are identified for $r_c = 1$, $\Omega_{mc} = 0$, $\Omega_{rc} = 0$, and $\lambda_c = A_{\pm}$ (refer to Appendix: A for the complete form of $A_{\pm}$). These fixed points exist for the potentials $V_1 - V_3$ and V_7. However, the values of θ_c are not the same for these points. These equilibrium points exist when
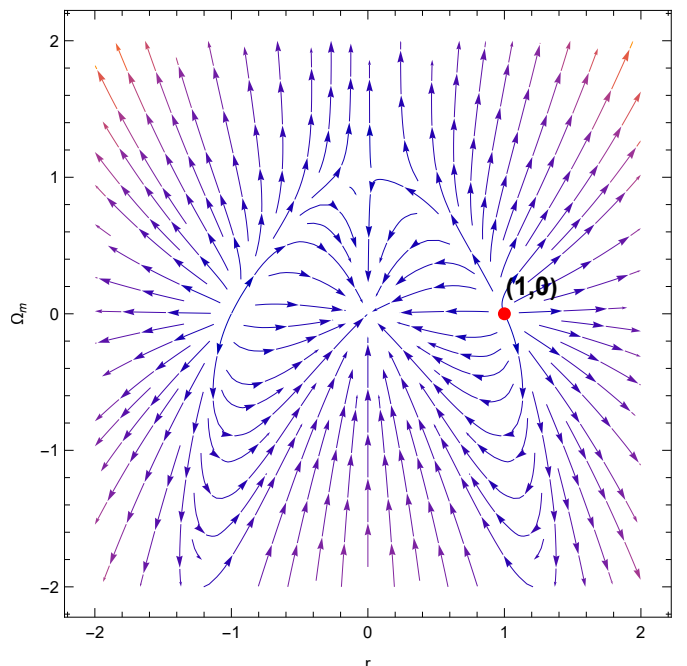

FIG. 1: Phase plot for the system of equations Eq.(9) in $(r - \Omega_m)$ plane for the fixed point e_2.

$\alpha_2 \neq 0$ and $\alpha_1^2 - 4\alpha_0\alpha_2 \geq 0$. The eigenvalues of $e3$ are determined by whether n is even or odd, while the eigenvalues of $e4_{\pm}$ are independent of n. In all cases, the Jacobian matrix evaluated at $e3$ and $e4_{\pm}$ exhibits positive eigenvalues. Consequently, the fixed points represented by $e3$ and $e4_{\pm}$ are unstable regardless of the values of n and the parameters α_0, α_1, and α_2. These fixed points represent a decelerating universe with $w_{\phi} = w_{tot} = 1$.

D. Λ - Dominated Era

The equilibrium points representing the cosmological constant or Λ-domination era are represented by $r_c = 0$, $\Omega_{mc} = 0$, and $\Omega_{rc} = 0$. These fixed points

Equilibrium points	r_c	θ_c	Ω_{mc}	Ω_{rc}	λ_c	Potentials
r	0	$\frac{n\pi}{2}$	0	1	λ	$V_1 - V_8$
m	0	$\frac{n\pi}{2}$	1	0	λ	$V_1 - V_8$
$e1$	1	$n\pi$	0	0	0	$V_2, V_6 - V_8$
$e2$	1	$n\pi \pm \frac{\pi}{2}$	0	0	0	$V_1 - V_8$
$e3$	1	$n\pi$	0	0	$A_\pm$	$V_1 - V_3, V_7$
$e4_\pm$	1	$n\pi \pm \cos^{-1}\left(\frac{A_\pm}{\sqrt{6}}\right)$	0	0	$A_\pm$	$V_1 - V_3, V_7$
c	0	$\frac{n\pi}{2}$	0	0	λ	$V_1 - V_8$
$er1_\pm$	$2E_\pm$	$2n\pi \pm \cos^{-1}\left(\sqrt{\frac{2}{3}}\right)$	0	$B_\pm$	$A_\mp$	V_1, V_3
$er2_\pm$	$-2E_\pm$	$(2n+1)\pi \pm \cos^{-1}\left(-\sqrt{\frac{2}{3}}\right)$	0	$B_\pm$	$A_\mp$	V_1, V_3
$er3_\pm$	$2E_\pm$	$2n\pi \pm \cos^{-1}\left(\sqrt{\frac{2}{3}}\right)$	0	$1 - 4E_\pm^2$	$\frac{1}{E_\pm}$	V_1, V_3
$er4_\pm$	$-2E_\pm$	$(2n+1)\pi \pm \cos^{-1}\left(-\sqrt{\frac{2}{3}}\right)$	0	$1 - 4E_\pm^2$	$\frac{1}{E_\pm}$	V_1, V_3
$er5_\pm$	$\pm\frac{2\alpha_2}{\alpha_1}$	$\left(n\pi \pm \cos^{-1}\left(\pm\sqrt{\frac{2}{3}}\right)\right)$	0	$1 - \frac{4\alpha_2^2}{\alpha_1^2}$	$-\frac{\alpha_1}{\alpha_2}$	V_2
$er6_\pm$	$\pm\frac{2\alpha_1}{\alpha_0}$	$\left(n\pi \pm \cos^{-1}\left(\pm\sqrt{\frac{2}{3}}\right)\right)$	0	$1 - \frac{4\alpha_1^2}{\alpha_0^2}$	$-\frac{\alpha_0}{\alpha_1}$	V_4
$em1_\pm$	$\sqrt{3}E_\pm$	$2n\pi \pm \frac{\pi}{4}$	$C_\pm$	0	$A_\mp$	V_1, V_3
$em2_\pm$	$-\sqrt{3}E_\pm$	$2n\pi \pm \frac{3\pi}{4}$	$C_\pm$	0	$A_\mp$	V_1, V_3
$em3_\pm$	$\pm\sqrt{3}E_\pm$	$n\pi \pm \frac{\pi}{4}$	$1 - 3E_\pm^2$	0	$\frac{1}{E_\pm}$	V_1, V_3
$em4$	$\frac{\sqrt{3}\alpha_2}{\alpha_1}$	$2n\pi \pm \frac{\pi}{4}$	$1 - \frac{3\alpha_2^2}{\alpha_1^2}$	0	$-\frac{\alpha_1}{\alpha_2}$	V_2
$em5$	$-\frac{\sqrt{3}\alpha_2}{\alpha_1}$	$2n\pi \pm \frac{3\pi}{4}$	$1 - \frac{3\alpha_2^2}{\alpha_1^2}$	0	$-\frac{\alpha_1}{\alpha_2}$	V_2
$em6$	$\frac{\sqrt{3}\alpha_1}{\alpha_0}$	$2n\pi \pm \frac{\pi}{4}$	$1 - \frac{3\alpha_1^2}{\alpha_0^2}$	0	$-\frac{\alpha_0}{\alpha_1}$	V_4
$em7$	$-\frac{\sqrt{3}\alpha_1}{\alpha_0}$	$2n\pi \pm \frac{3\pi}{4}$	$1 - \frac{3\alpha_1^2}{\alpha_0^2}$	0	$-\frac{\alpha_0}{\alpha_1}$	V_4
$ec1$	r	$n\pi \pm \frac{\pi}{2}$	0	0	0	$V_1 - V_8$
$ec2_\pm$	$\pm\frac{1}{\sqrt{2}}E_\pm D_\mp$	$n\pi,$ $2n\pi \pm \cos^{-1}\left(\frac{D_\mp}{2\sqrt{3}}\right)$	0	0	$A_\mp$	V_1, V_3

TABLE II: The list of equilibrium points for the system of equations given in Eq.(9). The complete expressions of $A_\pm, B_\pm, C_\pm, D_\pm E_\pm$ are given in Appendix-A. The last column of the table shows the classes of potentials for which the fixed points exist.

Equilibrium points	eigenvalues
r	$4, 3, -1, 1, 0$ for $\theta = n\pi$; $4, -3, 2, 1, 0$ for $\theta = n\pi \pm \frac{\pi}{2}$
m	$3, 3, -\frac{3}{2}, -1, 0$ for $\theta = n\pi$; $-3, 3, \frac{3}{2}, -1, 0$ for $\theta = n\pi \pm \frac{\pi}{2}$
$e1$	$6, 3, 3, 2, -\sqrt{6}\alpha_1$, for even n; $6, 3, 3, 2, +\sqrt{6}\alpha_1$, for odd n
$e2$	$-4, -3, 0, \frac{1}{2}\left(-3 + \sqrt{9 - 12\alpha_0}\right), \frac{1}{2}\left(-3 - \sqrt{9 - 12\alpha_0}\right)$
$e3$	$2, 3, 6, \mp\sqrt{6}\sqrt{\alpha_1^2 - 4\alpha_0\alpha_2}, 3 - \sqrt{\frac{3}{2}}A_\pm$, for even n; $2, 3, 6, \pm\sqrt{6}\sqrt{\alpha_1^2 - 4\alpha_0\alpha_2}, 3 + \sqrt{\frac{3}{2}}A_\pm$, for odd n
$e4_\pm$	$2, 3, 6, \mp\sqrt{6}\sqrt{\alpha_1^2 - 4\alpha_0\alpha_2}, 3 - \sqrt{\frac{3}{2}}A_\pm$
c	$-4, -3, -3, 3, 0$ for $\theta = n\pi$; $-4, -3, -3, 0, 0$ for $\theta = n\pi \pm \frac{\pi}{2}$
$er1_\pm, er2_\pm$	$1, 4, -8\alpha_2 - 4\alpha_1 E_\pm,$ $\frac{1}{2}\left(-1 \pm \frac{1}{\alpha_0}\sqrt{-\left(15\alpha_0^2 + 64\alpha_0\alpha_2 + 64\alpha_1\alpha_2 A_\pm\right)}\right),$
$er3_\pm, er4_\pm$	-
$er5_\pm$	$1, 4, -4\alpha_2, \frac{1}{2} \pm \left(\frac{1}{6\alpha_1}\right)\sqrt{3(3 - 8\sqrt{6})\alpha_1^2 + 96\sqrt{6}\alpha_2^2}$
$er6_\pm$	$1, 4, \frac{4\alpha_1^2}{\alpha_0}, \frac{1}{2} \pm \left(\frac{1}{6\alpha_0}\right)\sqrt{3(3 - 8\sqrt{6})\alpha_0^2 + 96\sqrt{6}\alpha_1^2}$
$em1_\pm, em2_\pm$	$-1, 3, -6\alpha_2 - 3\alpha_1 E_\pm,$ $\frac{3}{4}\left(-1 \pm \frac{1}{\alpha_0}\sqrt{-\left(7\alpha_0^2 + 24\alpha_0\alpha_2 + 24\alpha_1\alpha_2 A_\pm\right)}\right),$
$em3_\pm$	-
$em4, em5$	$-1, 3, -3\alpha_2, \frac{3}{4}\left(-1 \pm \left(\frac{3}{4\alpha_1}\right)\sqrt{24\alpha_2^2 - 7\alpha_1^2}\right)$
$em6, em7$	$-1, 3, \frac{3\alpha_1^2}{\alpha_0}, \frac{3}{4}\left(-1 \pm \left(\frac{3}{4\alpha_0}\right)\sqrt{24\alpha_1^2 - 7\alpha_0^2}\right)$
$ec1$	$-4, -3, 0, \frac{1}{2}\left(-3 \pm \sqrt{9 - 12\alpha_0 r_c^2}\right)$
$ec2_\pm$	$2, 3, 6, 3 \mp \frac{\sqrt{3}}{2}\sqrt{-\frac{2\alpha_0}{\alpha_2} - \frac{2\alpha_1}{\alpha_2}A_\mp},$ $\pm\frac{\sqrt{3}\alpha_2}{\alpha_0}A_\pm\sqrt{\alpha_1^2 - 4\alpha_0\alpha_2}\sqrt{-\frac{2\alpha_0}{\alpha_2} - \frac{2\alpha_1}{\alpha_2}A_\mp}$, for even n and $sin\theta = 0$; $2, 3, 6, 3 \pm \frac{\sqrt{3}}{2}\sqrt{-\frac{2\alpha_0}{\alpha_2} - \frac{2\alpha_1}{\alpha_2}A_\mp},$ $\mp\frac{\sqrt{3}\alpha_2}{\alpha_0}A_\pm\sqrt{\alpha_1^2 - 4\alpha_0\alpha_2}\sqrt{-\frac{2\alpha_0}{\alpha_2} - \frac{2\alpha_1}{\alpha_2}A_\mp}$, for odd n and $sin\theta = 0$; $2\alpha_0 + \alpha_1 A_\mp, -\frac{\alpha_0}{\alpha_2} - \left(\frac{\alpha_1}{\alpha_2}\right)A_\mp, -\frac{1}{\alpha_2}\left(\alpha_0 + 3\alpha_2\right) - \left(\frac{\alpha_1}{\alpha_2}\right)A_\mp,$ $-\frac{1}{\alpha_2}\left(\alpha_0 + 4\alpha_2\right) - \left(\frac{\alpha_1}{\alpha_2}\right)A_\mp, -\frac{1}{2\alpha_2}\left(\alpha_0 + 6\alpha_2\right) - \left(\frac{\alpha_1}{2\alpha_2}\right)A_\mp$, for $cos\theta = \frac{D_\mp}{2\sqrt{3}}$

TABLE III: The list of eigenvalues of the equilibrium points given in Table-*II*. For the fixed points $er3_\pm, er4_\pm, em3_\pm$ the analytical forms of the eigenvalues are complicated and hence not included in the table. These eigenvalues can be computed for some particular choices of α parameters, see the text for more details.

exist for all potentials listed in Table-*I*. In this case, the equilibrium points are given by 'c' in the Table-*II* and they are nonisolated equilibrium points. The eigenvalues of the Jacobian matrix evaluated at 'c' depend on θ_c. For $\theta_c = n\pi$ the Jacobian matrix has a mixture of positive and negative eigenvalues, hence the fixed points in this case are saddle. On the other hand, finding the stability of the equilibrium points 'c' for $\theta_c = n\pi \pm \frac{\pi}{2}$ is more involved since it has two zero eigenvalues and other all negative eigenvalues. Three negative eigenvalues correspond to a 3D stable manifold, whereas the two zero eigenvalues correspond to a 2D center manifold. In general, one can use the center manifold theorem to investigate the stability of this fixed point, rather here we draw the phase plots on 3D planes. All the points in red color and the points on the lines shown in red in the projected phase spaces, as depicted in Fig. 2, represent

Equilibrium points	q	ω_ϕ	ω_{tot}
r	1	1 for $\theta = n\pi$; -1 for $\theta = n\pi \pm \frac{\pi}{2}$	$\frac{1}{3}$
m	$\frac{1}{2}$	1 for $\theta = n\pi$; -1 for $\theta = n\pi \pm \frac{\pi}{2}$	0
$e1, e3, e4_\pm$	2	1	1
$e2$	-1	-1	-1
c	-1	1 for $\theta = n\pi$; -1 for $\theta = n\pi \pm \frac{\pi}{2}$	-1
$er1_\pm, er2_\pm,$ $er3_\pm, er4_\pm$	$\frac{\alpha_0^2 + 16\alpha_2\alpha_0 + 8\left(\sqrt{\alpha_1^2 - 4\alpha_0\alpha_2} - \alpha_1\right)\alpha_1}{\alpha_0^2}$, for er_+ $\frac{\alpha_0^2 + 16\alpha_2\alpha_0 - 8\alpha_1\left(\sqrt{\alpha_1^2 - 4\alpha_0\alpha_2} + \alpha_1\right)}{\alpha_0^2}$, for er_-	$\frac{1}{3}$	$\frac{1}{3}$
$er5_\pm, er6_\pm$	$1 - \frac{16\alpha_1^2}{\alpha_0^2}$, for $er5_\pm$; $1 - \frac{16\alpha_2^2}{\alpha_1^2}$, for $er6_\pm$	$\frac{1}{3}$	$\frac{1}{3}$
$em1_\pm,$ $em2_\pm, em3_\pm$	$\frac{\alpha_0^2 + 18\alpha_2\alpha_0 + 9\left(\sqrt{\alpha_1^2 - 4\alpha_0\alpha_2} - \alpha_1\right)\alpha_1}{2\alpha_0^2}$, for em_+ $\frac{\alpha_0^2 + 18\alpha_2\alpha_0 - 9\alpha_1\left(\sqrt{\alpha_1^2 - 4\alpha_0\alpha_2} + \alpha_1\right)}{2\alpha_0^2}$, for em_-	$\frac{1}{3}$	$\frac{1}{3}$
$em4, em5$	$\frac{1}{2} - \frac{9\alpha_2^2}{\alpha_1^2}$	0	0
$em6, em7$	$\frac{1}{2} - \frac{9\alpha_1^2}{\alpha_0^2}$	0	0
$ec1$	-1	-1	-1
$ec2_\pm$	-4, for $\theta = n\pi$; $\frac{2(\alpha_0 - 2\alpha_2)\alpha_2 - \alpha_1\left(\sqrt{\alpha_1^2 - 4\alpha_0\alpha_2} + \alpha_1\right)}{4\alpha_2^2}$, for $r_c = \pm\frac{1}{\sqrt{2}}E_+D_-$ $\frac{\left(\sqrt{\alpha_1^2 - 4\alpha_0\alpha_2} - \alpha_1\right)\alpha_1 + 2\alpha_2(\alpha_0 - 2\alpha_2)}{4\alpha_2^2}$, for $r_c = \pm\frac{1}{\sqrt{2}}E_-D_+$	1, for $\theta = n\pi$; $\frac{\alpha_1\left(\sqrt{\alpha_1^2 - 4\alpha_0\alpha_2} + \alpha_1\right) - 2\alpha_2(\alpha_0 + 3\alpha_2)}{6\alpha_2^2}$, for $r_c = \pm\frac{1}{\sqrt{2}}E_+D_-$ $\frac{\alpha_1^2 - \sqrt{\alpha_1^2 - 4\alpha_0\alpha_2}\alpha_1 - 2\alpha_2(\alpha_0 + 3\alpha_2)}{6\alpha_2^2}$, for $r_c = \pm\frac{1}{\sqrt{2}}E_-D_+$	1, for $\theta = n\pi$; $\frac{\alpha_1\left(\sqrt{\alpha_1^2 - 4\alpha_0\alpha_2} + \alpha_1\right) - 2\alpha_2(\alpha_0 + 3\alpha_2)}{6\alpha_2^2}$, for $r_c = \pm\frac{1}{\sqrt{2}}E_+D_-$ $\frac{\alpha_1^2 - \sqrt{\alpha_1^2 - 4\alpha_0\alpha_2}\alpha_1 - 2\alpha_2(\alpha_0 + 3\alpha_2)}{6\alpha_2^2}$, for $r_c = \pm\frac{1}{\sqrt{2}}E_-D_+$

TABLE IV: The values of cosmological parameters for the equilibrium points given in Table-II.

the equilibrium point 'c' for the V_2 potential. From this figure, we can see that the fixed points given by 'c' are stable for $\theta = n\pi \pm \frac{\pi}{2}$ in all projected subspaces and hence stable in the entire 5D space. We have also checked that for the other class of potentials, the behaviour of the fixed point remains the same. These fixed points represent an accelerating universe with $w_\phi = 1$ and $w_{tot} = -1$ for $\theta = n\pi$ whereas $w_\phi = w_{tot} = -1$ for $\theta = n\pi \pm \frac{\pi}{2}$. Interestingly, in the first case, the scalar field behaves as a stiff fluid.

E. The Era Shared by Scalar Field and other components

In our setup, there are some specific fixed points that indicate scenarios where the energy budget is shared between the scalar field and other components.

The Era Shared by the Scalar Field and Radiation

The fixed points $er1_\pm$ to $er6_\pm$ represent the state where the universe's energy budget is shared by radiation and the scalar field by the relation $r_c^2 + \Omega_{rc} = 1$. These equilibrium points are detailed in the Table-II. For each $n \in \mathbb{Z}$, the equilibrium points $er1_\pm$, $er2_\pm$, $er5_\pm$, and $er6_\pm$ exhibit positive eigenvalues, making these points unstable or saddle depending on the choice of parameters $\alpha_0, \alpha_1, \alpha_2$. The eigenvalues of the Jacobian matrix at $er3_\pm$ and $er4_\pm$ are complicated in general, making it difficult to draw any conclusions about their stability. For these points, we evaluate the stability at specific values of α parameters. We have considered the same value of the α parameters that have been used to plot Fig.4 and Fig.6, for potentials V_1 and V_3 respectively. For the potential V_1 the eigenvalues at $er3_\pm$ are $1, 4, -2.8394$, and $-0.5 \pm 1.93041i$, while at $er4_\pm$ they are $-201.793, -11.2262, 10.2262, 4$, and 1, indicating that these points are saddle points. For potential V_3, the eigenvalues at $er3_\pm$ and $er4_\pm$ are $1, 4, -4.48$, and $-0.5 \pm 1.92544i$, showing that they are saddle points. The fixed points $er1_\pm$ and $er2_\pm$
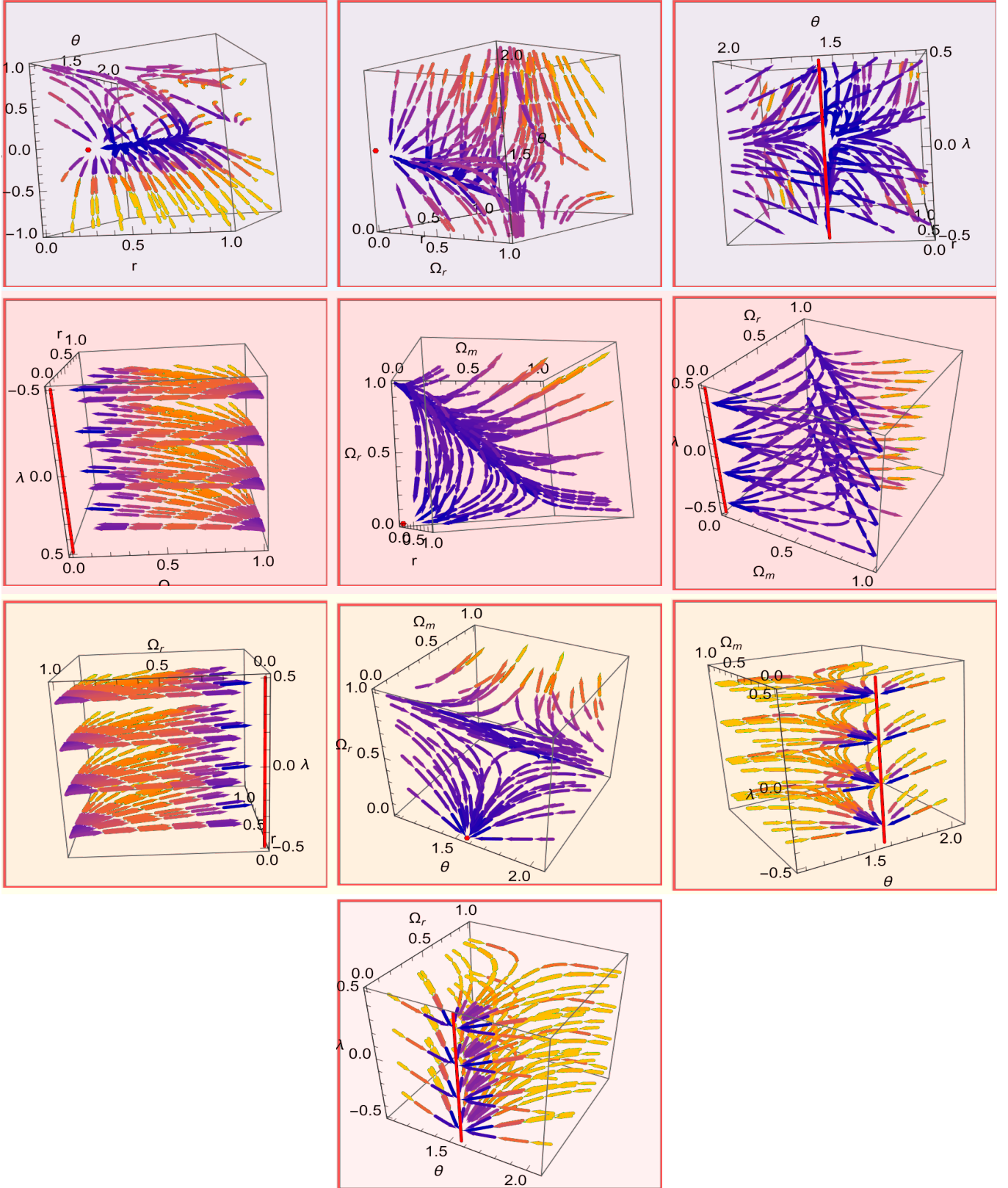
FIG. 2: Phase plots in different $3D$ projected spaces for the equilibrium point 'c' and for the potential V_2.

exist for the potentials V_1 and V_3; $er5_\pm$ exist for the potential V_2; and $er6_\pm$ for potential V_4. For all possible equilibrium points in this era $w_\phi = w_{tot} = 1/3$ representing a decelerated universe.

The Era Shared by the Scalar Field and Matter

For the equilibrium points in the era shared by scalar field and matter, we have $r_c^2 + \Omega_{mc} = 1$. In this case, the equilibrium points are given by $em1_\pm$ - $em7$ and are given in Table-*II*. For each $n \in \mathbb{Z}$, though the eigenvalues of the Jacobian matrix eval-
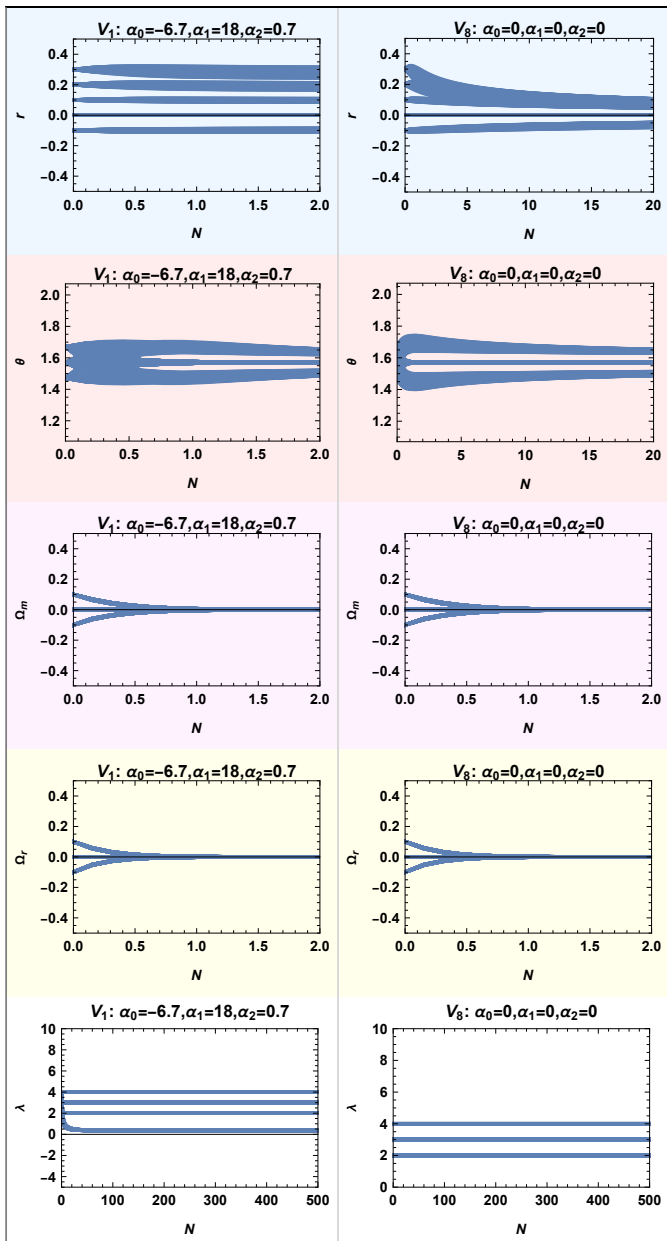
FIG. 3: Plots of the numerical solutions for each dynamical variable by considering perturbations around the equilibrium point $ec1$. The plots in the left column are shown for potential V_1 and on the right it is shown for the potential V_8.

uated at the equilibrium points $em1_\pm$, $em2_\pm$ and $em4 - em7$ depend on the parameters α_0, α_1 and α_2; but it has a positive eigenvalue irrespective of α_i. So, the equilibrium points given in this era are unstable in nature. The equilibrium points $em1_\pm - em3_\pm$ exist for the potentials V_1, V_3; $em4$ and $em5$ exist for the potential V_2; $em6$ and $em7$ exist for the potential V_4. The eigenvalues of the Jacobian matrix evaluated at the equilibrium points $em3_\pm$ are very complicated. So, for $em3_\pm$, we evaluate the stability similarly as the case for $er3_\pm$ and $er4_\pm$. For the potential V_1 the eigenvalues at $em3_+$ are $3, -1, -2.12955$, and $-0.75 \pm 1.97931i$, while at $er3_-$ they are $9.06334, 3, -1, -10.5633$, and -151.345, in-

dicating that these points are saddle points. For potential V_3, the eigenvalues at $em3_\pm$ are $3, -1, -3.36$, and $-0.75 \pm 1.97522i$, showing that they are saddle points. The exact value of the deceleration parameter depends on α parameters for all the potentials belonging to this era. However, for all possible equilibrium points in this era $w_\phi = w_{tot} = 0$ representing a decelerated universe.

The Era Shared by the Scalar Field and Λ

For the equilibrium points in the era shared by scalar field and Λ, we have $r_c^2 + \Omega_{\Lambda c} = \Omega_{\phi c} + \Omega_{\Lambda c} = 1$. In this case, the equilibrium points are given by $ec1$ and $ec2_\pm$. The equilibrium points given by $ec1$ exist for all potentials $V_1 - V_8$. Those equilibrium points are given in the Table-II. The nature of the equilibrium points given by $ec1$ depends on the parameter α_0. If $0 < \alpha_0 < \frac{3}{4r_c^2}$, then the equilibrium points given by $ec1$ are normally hyperbolic equilibrium points and the Jacobian matrix has four eigenvalues with negative real part and one zero eigenvalues. Again, if $\alpha_0 = 0$ then the equilibrium points given by $ec1$ are of non-hyperbolic type and the Jacobian matrix has three negative and two zero eigenvalues. To check the stability of those equilibrium points we plot the evolution of the dynamical variables $r, \theta, \Omega_m, \Omega_r$ and λ by solving the system numerically where the system has been perturbed from the equilibrium point $ec1$. This approach for finding the stability of the non-hyperbolic fixed points has been previously used in [41–43]. In Fig.3 for example we have plotted the evolution of the system with N for the potentials V_1 (on the left column) and V_8 (on the right column) subjected to perturbations around the fixed point ec_1. We can see that the evolution of the dynamical variables does not diverge but rather stays in the neighbourhood of the fixed point, indicating its stable nature. We have also checked that the qualitative behaviour of the fixed point remains the same even for the other potentials. Thus, the fixed points given by $ec1$ are stable for $\alpha_0 = 0$. Again, if $\alpha_0 < 0$, then the equilibrium points given by $ec1$ are non-hyperbolic type and the Jacobian matrix has a positive eigenvalue. Thus, the equilibrium points given by $ec1$ are stable for $0 \leq \alpha_0 \leq \frac{3}{4r_c^2}$, where $0 \leq r_c \leq 1$ and unstable for $\alpha_0 < 0$. These fixed points represent an accelerating universe with $w_\phi = w_{tot} = -1$.

The equilibrium points $ec2_\pm$ are defined by $r_c = \pm\frac{1}{\sqrt{2}}E_\pm D_\mp$, $\Omega_{mc} = 0$, $\Omega_{rc} = 0$, and $\lambda_c = A_\mp$ and exists for potentials V_1 and V_3. There are two distinct types of θ_c at these points: $\theta_c = n\pi$ and $\theta_c = 2n\pi \pm \cos^{-1}\frac{D_\mp}{2\sqrt{3}}$. For $\theta_c = n\pi$, the eigenvalues of the Jacobian matrix vary depending on whether n is even or odd, but some eigenvalues are always

positive, hence the fixed points are unstable. For $\theta_c = 2n\pi \pm \cos^{-1} \frac{D_\mp}{2\sqrt{3}}$, the form of the eigenvalues is complicated and it is not possible to conclude stability analytically for this fixed point for any general choice of the parameters α. Thus, stability was assessed for specific values of the parameters α_0, α_1, and α_2 that are considered for the numerical solutions shown in Fig.1 and Fig.3. The Jacobian matrix has at least one positive eigenvalue for our choices of the α parameters, making $ec2_\pm$ unstable. These points also correspond to an accelerating universe.

VI. EDE LIKE BEHAVIOR OF THE SCALAR FIELD

In our analysis of the phase space for the current model, which includes a nonminimally coupled scalar field and the cosmological constant as potential candidates for dark energy, we observed that there is no late-time attractor completely dominated by the scalar field. The only possible late-time attractors are either completely dominated by the cosmological constant or a scenario where there is only the cosmological constant and scalar field present in the universe, the rest of the components are absent. Although there are epochs where the scalar field and other components coexist, these correspond to the fixed points, which are saddle or unstable.

In the following, we aim to explore the possibility of the scalar field contributing to the universe's energy budget prior to the onset of the dark energy dominated epoch. This is motivated by the presence of fixed points in the system that corresponds to the eras that might be potentially shared between other components and the scalar field, suggesting an early dark energy (EDE) like behaviour of the scalar field.

The EDE models predict that the dark energy makes up approximately 10% of the universe's energy budget just before or during the recombination era. Identifying early dark-energy-like solutions is quite challenging, as the solutions are highly sensitive to the initial conditions. In this study, we numerically solve the system of equations Eq.(9) by considering the specific initial conditions given in Table-VI. In particular, except for the initial condition of λ for all potentials, the initial conditions for the other variables remain almost the same. The initial condition is set before the radiation-matter equality at $N = -10.1$, corresponding to $z \approx 22026$, deep in the radiation-dominated era. The range of α parameters and λ_{ini} for each class of potential is presented in Table-I, for which the qualitative behaviour of our analysis remains the same.

The evolution of the density parameters for various components of the universe corresponding to all the classes of potentials are shown in Fig.4 to Fig.11 respectively. For the classes of potentials, V_1 - V_6 we can see the EDE like behaviour of the scalar field appears naturally in the deep-matter dominated era, which is almost 10% of the total energy budget of the universe. But, at present the contribution of the scalar field is negligible. Whereas for the classes of potentials, V_7 and V_8 also the similar behaviour of the scalar field appears naturally in the deep matter-dominated era, which is almost 10% of the total energy budget of the universe. Contrary to the previous case for these two classes of potentials at present as well as near future the scalar field has a non-negligible contribution to the total energy budget of the universe. The redshift parameter values for matter-radiation equality and the occurrence of EDE-like behavior of the scalar field are provided in Table-VI for the numerical solutions obtained for all classes of potentials.

We have also plotted the evolution of different cosmological parameters like the deceleration parameter in Fig.12, the equation of state of the scalar field in Fig.13 and the total equation of state in Fig.14 for all potentials. Those plots are drawn for the same values of the parameters α for which Fig.4 to Fig.11 are drawn. For the evolution of the deceleration parameter, one can see that its value has become negative in the recent past from positive, showing the accelerating expansion of the universe. It can be seen that the transition of the universe from the decelerated to accelerated phase remains smooth throughout except for the epoch where the scalar field shows EDE like behaviour. During this epoch, the deceleration parameter shows some increments suggesting more deceleration of the universe due to the activation of the scalar field. Later, it started to decrease and become negative with time. From the plot of the EOS of the scalar field in Fig.13 one can see that in the very early universe, the scalar field behaves like a stiff fluid with EOS $w_\phi = 1$ then it becomes $w_\phi = -1$. During the EDE like behaviour of the scalar field, it increases and becomes positive and the scalar field does not contribute to the acceleration of the universe since $w_\phi > -1/3$ rather it was slowing down the expansion of the universe. This can also be seen from the plot of the w_{tot} in Fig.14 since during this epoch the w_{tot} becomes positive and starts to decrease again.

In Fig.15 we have shown the evolution of the $H(z)$ vs z for all the classes of potentials we have considered here. It can be seen that these potentials fit the data quite well, at least during the late time evolution. We acknowledge that a comprehensive parameter estimation using current cosmological data is necessary to constrain the parameters and comment more accurately on this EDE like behaviour of the scalar field, which is beyond the scope of the current

work. This will be addressed in future research.

VII.   CONCLUSION

In this study, we explore the dynamics and phase-space characteristics of a multicomponent dark energy model. This model features a dark sector that includes a minimally coupled canonical scalar field and a cosmological constant. The equations are transformed into autonomous systems and subsequently into a polar form. We have considered a parameterization for the potentials of the scalar field that helps us to study a broad spectrum of potentials in a single setup.

By using dynamical system analysis, we find several fixed points that correspond to various cosmological eras together with possible late-time attractors. In this model, the late-time attractors are either completely dominated by the cosmological constant or present a scenario where both the scalar field and the cosmological constant coexist, excluding all other components.

We also investigated numerically the possibility of EDE like behaviour for all the different classes of potentials considered in this work and observed that this EDE like behaviour of the scalar field occurs deep within the matter-dominated era, not near the recombination period. We also found that during this EDE like era of the scalar field, it behaves more like matter rather than dark energy. During this era, the universe becomes more decelerated compared to the standard case. The total EOS of the universe also shows a transition from negative to positive values during this epoch. A detailed examination of this EDE like behaviour of the scalar field will require a comprehensive cosmological data analysis with the recent data, which we will present in the future.
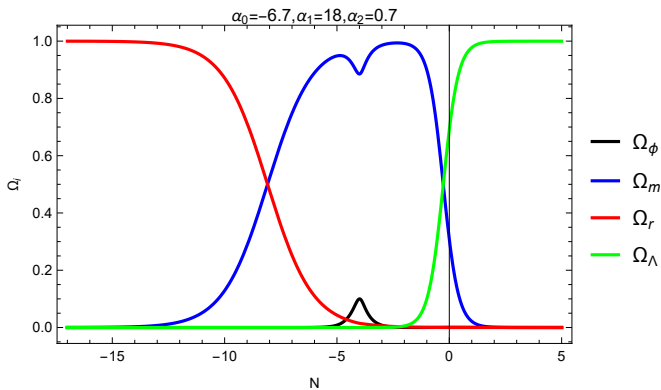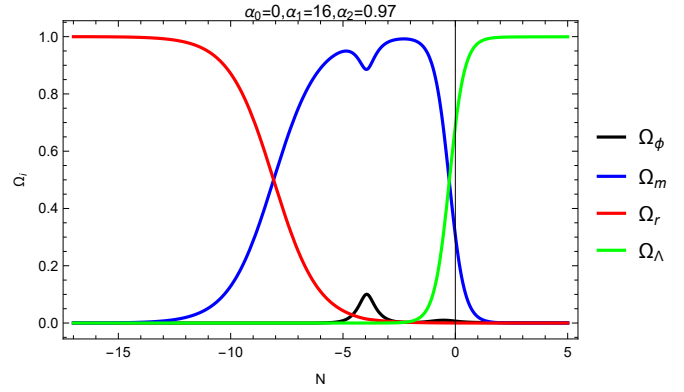

FIG. 5: Plot of the density parameters for different components of universe for the potential V_2.
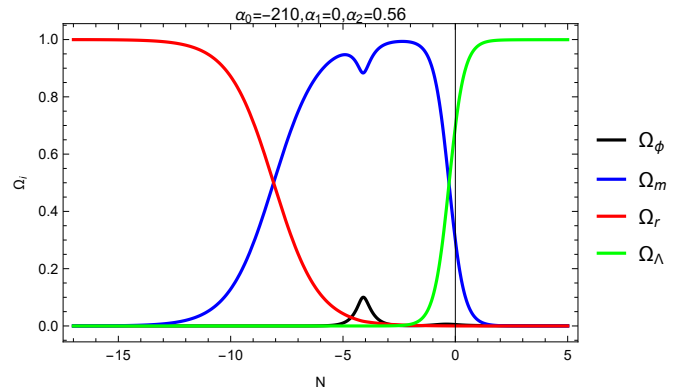

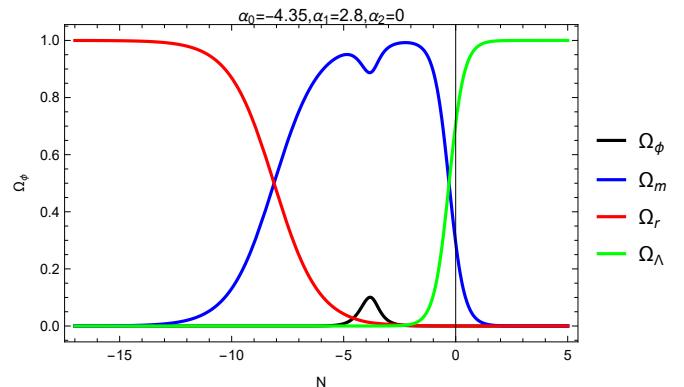FIG. 6: Plot of the density parameters for different components of universe for the potential V_3.

FIG. 4: Plot of the density parameters for different components of universe for the potential V_1.

FIG. 7: Plot of the density parameters for different components of universe for the potential V_4.

Potentials	N_{ini}	r_{ini}	θ_{ini}	$\Omega_{m_{ini}}$	$\Omega_{r_{ini}}$	λ_{ini}
V_1	-10.1	$\sqrt{0.3 \times 10^{-9}}$	$tan^{-1}(-2)$	$0.118 - \frac{(r_{ini})^2}{2}$	$0.882 - \frac{(r_{ini})^2}{2}$	-2.4
V_2	-10.1	$\sqrt{0.3 \times 10^{-9}}$	$tan^{-1}(-2)$	$0.118 - \frac{(r_{ini})^2}{2}$	$0.882 - \frac{(r_{ini})^2}{2}$	-2.93
V_3	-10.1	$\sqrt{0.36 \times 10^{-9}}$	$tan^{-1}(-2)$	$0.118 - \frac{(r_{ini})^2}{2}$	$0.882 - \frac{(r_{ini})^2}{2}$	-0.64
V_4	-10.1	$\sqrt{0.3 \times 10^{-9}}$	$tan^{-1}(-2)$	$0.118 - \frac{(r_{ini})^2}{2}$	$0.882 - \frac{(r_{ini})^2}{2}$	-4.49
V_5	-10.1	$\sqrt{0.3 \times 10^{-9}}$	$tan^{-1}(-2)$	$0.118 - \frac{(r_{ini})^2}{2}$	$0.882 - \frac{(r_{ini})^2}{2}$	-5.13
V_6	-10.1	$\sqrt{0.3 \times 10^{-9}}$	$tan^{-1}(-2)$	$0.118 - \frac{(r_{ini})^2}{2}$	$0.882 - \frac{(r_{ini})^2}{2}$	-5.785
V_7	-10.1	$\sqrt{0.3 \times 10^{-9}}$	$tan^{-1}(-2)$	$0.118 - \frac{(r_{ini})^2}{2}$	$0.882 - \frac{(r_{ini})^2}{2}$	-6
V_8	-10.1	$\sqrt{0.3 \times 10^{-9}}$	$tan^{-1}(-2)$	$0.118 - \frac{(r_{ini})^2}{2}$	$0.882 - \frac{(r_{ini})^2}{2}$	-6.59

TABLE V: The initial values of the variables for which the numerical solution of the system of equations Eq.(9) has been obtained.

Potentials	λ_{ini}	α_0	α_1	α_2	z_{eq}	z_*
V_1	$[-2.5, -2.4]$	$[-20, -4.65]$	$[18, 20]$	$[0.4, 0.7]$	3228	54
V_2	$[-3, -2.93]$	0	$[16, 20]$	$[0.9, 1]$	3228	52
V_3	$[-0.7, -0.5]$	$[-270, -200]$	0	$[0.47, 0.8]$	3228	58
V_4	$[-4.6, -4.49]$	$[-8, -4.35]$	$[2.8, 3]$	0	3293	43
V_5	$[-5.3, -5.13]$	$[-16.5, -12]$	0	0	3228	44
V_6	$[-5.9, -5.785]$	0	$[0.9, 1.1]$	0	3228	40
V_7	$[-6.1, -5.99]$	0	0	$[-0.15, -0.1]$	3228	38
V_8	$[-6.9, -6.59]$	0	0	0	3228	31

TABLE VI: The range of parameters and λ_{ini} for which the qualitative behavior of the numerical solution of the system of equations Eq. (9) remains unchanged.
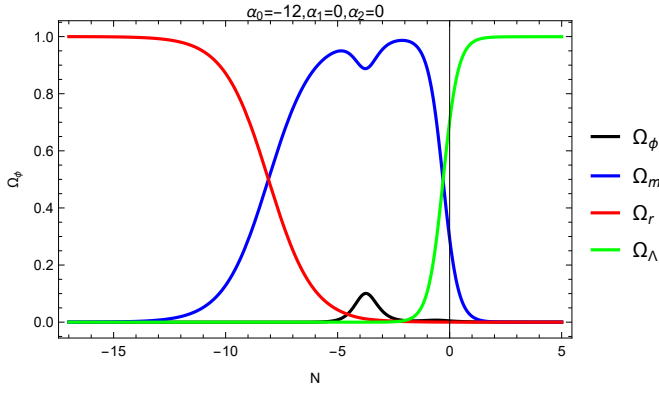
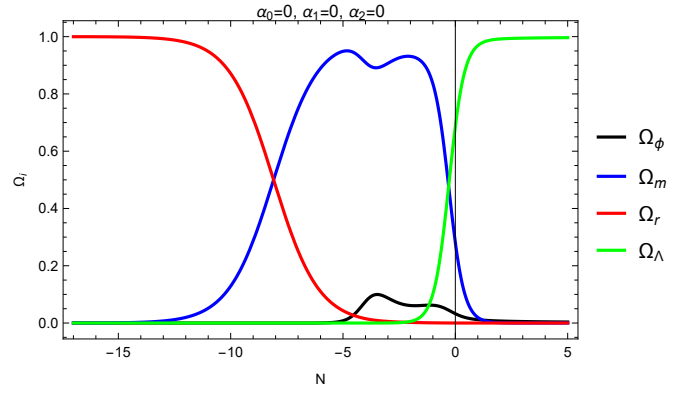FIG. 8: Plot of the density parameters for different components of universe for the potential V_5.

FIG. 11: Plot of the density parameters for different components of universe for the potential V_8.
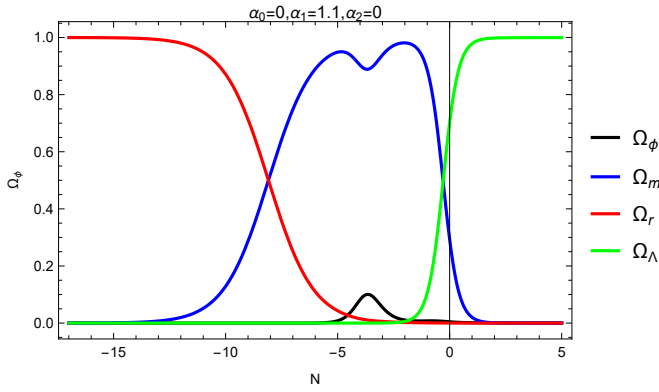

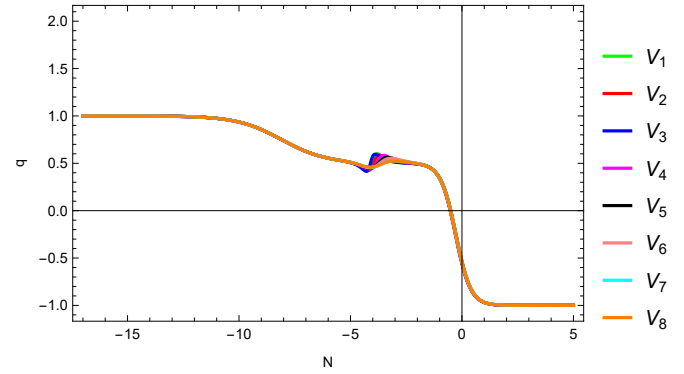FIG. 9: Plot of the density parameters for different components of universe for the potential V_6.

FIG. 12: Plots of the deceleration parameter for early dark energy with respect to different classes of potentials.
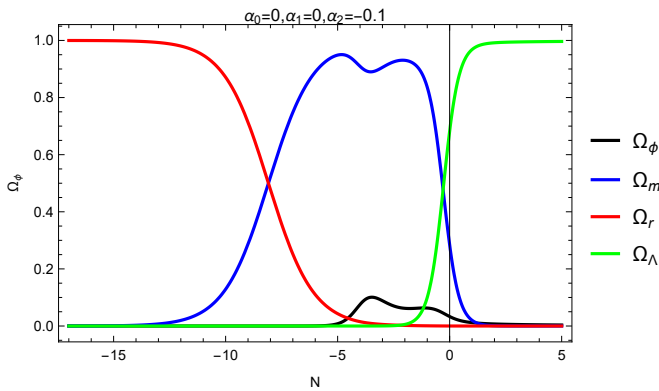

FIG. 10: Plot of the density parameters for different components of universe for the potential V_7.
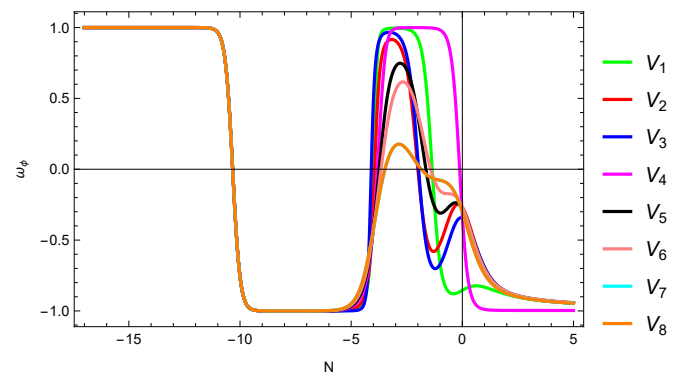

FIG. 13: Plots of the equation of state for scalar field for different classes of potentials.
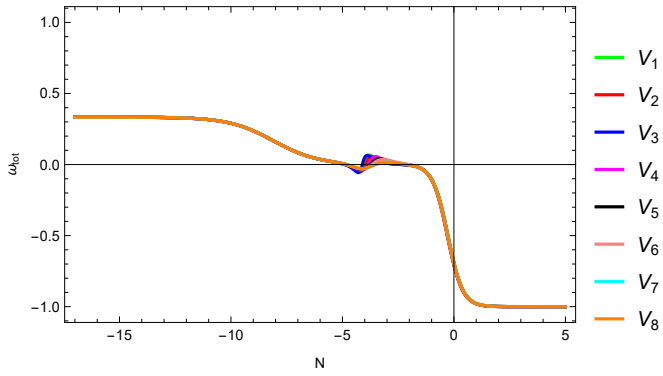
FIG. 14: Plots of the total equation of state with respect to different classes of potentials.
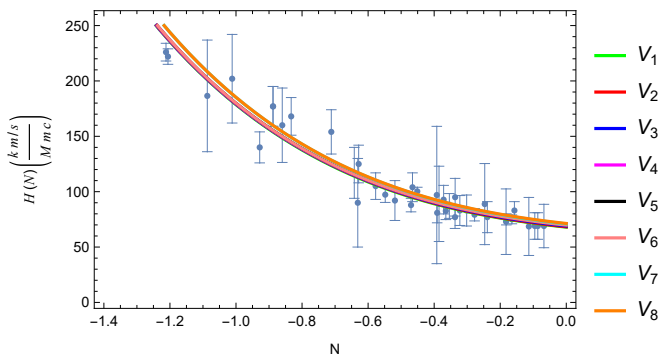

FIG. 15: Plot of the evaluation of the Hubble parameter $H(N)$ versus N for different classes of potentials. The data from various observations are also included for comparison.

Appendix A

$$A_\pm = \frac{-\alpha_1 \pm \sqrt{\alpha_1^2 - 4\alpha_0\alpha_2}}{2\alpha_2}.$$

$$E_\mp = \frac{-\alpha_1 \pm \sqrt{\alpha_1^2 - 4\alpha_0\alpha_2}}{2\alpha_0},$$

$$B_\pm = 1 + \frac{4\alpha_2}{\alpha_0} + \frac{4\alpha_1}{\alpha_0}E_\pm,$$

$$C_\pm = 1 + \frac{3\alpha_2}{\alpha_0} + \frac{3\alpha_1}{\alpha_0}E_\pm,$$

$$D_\mp = \sqrt{-\frac{2}{\alpha_2}\left(\alpha_1 A_\mp + \alpha_0\right)}.$$

Appendix B: Observed data for the Hubble's parameter vs. redshift & the e-folding.

z	$N = \ln(\frac{1}{1+z})$	$H(z)\left(\frac{\text{km/s}}{\text{Mpc}}\right)$	Ref.
0.07	-0.067	69 ± 19.6	[44]
0.09	-0.086	69 ± 12	[45]
0.100	-0.095	69 ± 12	[45]
0.120	-0.113	68.6 ± 26.2	[44]
0.170	-0.157	83 ± 8	[45]
0.179	-0.164	75 ± 4	[46]
0.199	-0.181	75 ± 5	[46]
0.200	-0.182	72.9 ± 29.6	[44]
0.270	-0.239	77 ± 14	[45]
0.280	-0.246	88.8 ± 36.6	[44]
0.320	-0.277	79.2 ± 5.6	[47]
0.352	-0.301	83 ± 14	[46]
0.3802	-0.322	83 ± 13.5	[46]
0.400	-0.336	95 ± 17	[45]
0.4004	-0.336	77 ± 10.2	[46]
0.4247	-0.353	87.1 ± 11.2	[46]
0.440	-0.364	82.6 ± 7.8	[48]
0.4497	-0.371	92.8 ± 12.9	[46]
0.470	-0.385	89 ± 34	[49]

z	$N = \ln(\frac{1}{1+z})$	$H(z)\left(\frac{\text{km/s}}{\text{Mpc}}\right)$	Ref.
0.4783	-0.390	80.9 ± 9	[46]
0.480	-0.392	97 ± 62	[50]
0.570	-0.451	100.3 ± 3.7	[47]
0.593	-0.465	104 ± 13	[46]
0.600	-0.470	87.9 ± 6.1	[48]
0.680	-0.518	92 ± 8	[46]
0.730	-0.548	97.3 ± 7	[48]
0.781	-0.577	105 ± 12	[46]
0.875	-0.628	125 ± 17	[46]
0.880	-0.631	90 ± 40	[50]
0.900	-0.641	117 ± 23	[45]
1.037	-0.711	154 ± 20	[46]
1.300	-0.832	168 ± 17	[45]
1.363	-0.859	160 ± 33.6	[51]
1.430	-0.887	177 ± 18	[45]
1.530	-0.928	140 ± 14	[45]
1.750	-1.011	202 ± 40	[45]
1.965	-1.086	186.5 ± 50.4	[51]
2.340	-1.205	222 ± 7	[52]
2.360	-1.211	226 ± 8	[53]

TABLE VII: Observed data for $H(z)$ as a function of z alongside the associated value of N, with references that have been used in this study.

[1] Adam G. Riess et al. Observational evidence from supernovae for an accelerating universe and a cosmological constant. *Astron. J.*, 116:1009–1038, 1998.

[2] S. Perlmutter et al. Measurements of Ω and Λ from 42 high redshift supernovae. *Astrophys. J.*, 517:565–586, 1999.

[3] Attila Meszaros. On the Reality of the accelerating universe. *Astrophys. J.*, 580:12–15, 2002.

[4] M. Arnaud et al. Planck intermediate results. XXXI. Microwave survey of Galactic supernova remnants. *Astron. Astrophys.*, 586:A134, 2016.

[5] Christopher P Ahn, Rachael Alexandroff, Carlos Allende Prieto, Scott F Anderson, Timothy Anderton, Brett H Andrews, Éric Aubourg, Stephen Bailey, Ed-

uardo Balbinot, Rory Barnes, et al. The ninth data release of the sloan digital sky survey: first spectroscopic data from the sdss-iii baryon oscillation spectroscopic survey. *The Astrophysical Journal Supplement Series*, 203(2):21, 2012.

[6] T Padmanabhan. Dark energy: mystery of the millennium. In *AIP Conference Proceedings*, volume 861, pages 179–196. American Institute of Physics, 2006.

[7] N. Aghanim et al. Planck 2018 results. VI. Cosmological parameters. *Astron. Astrophys.*, 641:A6, 2020. [Erratum: Astron.Astrophys. 652, C4 (2021)].

[8] Shadab Alam, Metin Ata, Stephen Bailey, Florian Beutler, Dmitry Bizyaev, Jonathan A. Blazek, Adam S. Bolton, Joel R. Brownstein, Angela Burden, Chia-Hsun Chuang, and et al. The clustering of galaxies in the completed sdss-iii baryon oscillation spectroscopic survey: cosmological analysis of the dr12 galaxy sample. *Monthly Notices of the Royal Astronomical Society*, 470(3):2617–2652, Mar 2017.

[9] Florian Beutler, Chris Blake, Matthew Colless, D. Heath Jones, Lister Staveley-Smith, Lachlan Campbell, Quentin Parker, Will Saunders, and Fred Watson. The 6df galaxy survey: baryon acoustic oscillations and the local hubble constant. *Monthly Notices of the Royal Astronomical Society*, 416(4):3017–3032, Jul 2011.

[10] Shadab Alam, Marie Aubert, Santiago Avila, Christophe Balland, Julian E. Bautista, Matthew A. Bershady, Dmitry Bizyaev, Michael R. Blanton, Adam S. Bolton, Jo Bovy, and et al. Completed sdss-iv extended baryon oscillation spectroscopic survey: Cosmological implications from two decades of spectroscopic surveys at the apache point observatory. *Physical Review D*, 103(8), Apr 2021.

[11] T. M. C. Abbott et al. Dark Energy Survey year 1 results: Cosmological constraints from galaxy clustering and weak lensing. *Phys. Rev. D*, 98(4):043526, 2018.

[12] E. Macaulay et al. First Cosmological Results using Type Ia Supernovae from the Dark Energy Survey: Measurement of the Hubble Constant. *Mon. Not. Roy. Astron. Soc.*, 486(2):2184–2196, 2019.

[13] E. Krause et al. Dark Energy Survey Year 1 Results: Multi-Probe Methodology and Simulated Likelihood Analyses. 6 2017.

[14] Adam G. Riess, Stefano Casertano, Wenlong Yuan, Lucas M. Macri, and Dan Scolnic. Large magellanic cloud cepheid standards provide a 1% foundation for the determination of the hubble constant and stronger evidence for physics beyond λcdm. *The Astrophysical Journal*, 876(1):85, May 2019.

[15] Kenneth C. Wong et al. H0LiCOW – XIII. A 2.4 percent measurement of H0 from lensed quasars: 5.3σ tension between early- and late-Universe probes. *Mon. Not. Roy. Astron. Soc.*, 498(1):1420–1439, 2020.

[16] Adam G. Riess, Louise Breuval, Wenlong Yuan, Stefano Casertano, Lucas M. Macri, J. Bradley Bowers, Dan Scolnic, Tristan Cantat-Gaudin, Richard I. Anderson, and Mauricio Cruz Reyes. Cluster cepheids with high precision gaia parallaxes, low zero-point uncertainties, and hubble space telescope photome-

try. *The Astrophysical Journal*, 938(1):36, oct 2022.

[17] Luca Amendola and Shinji Tsujikawa. *Dark energy: theory and observations*. Cambridge University Press, 2010.

[18] Kazuharu Bamba, Salvatore Capozziello, Shin'ichi Nojiri, and Sergei D. Odintsov. Dark energy cosmology: the equivalent description via different theoretical models and cosmography tests. *Astrophys. Space Sci.*, 342:155–228, 2012.

[19] Edmund J Copeland, Mohammad Sami, and Shinji Tsujikawa. Dynamics of dark energy. *International Journal of Modern Physics D*, 15(11):1753–1935, 2006.

[20] P. J. E. Peebles and B. Ratra. Quintessence: A review. *Reviews of Modern Physics*, 75(2):559–606, 2003.

[21] C. Armendariz-Picon, V. Mukhanov, and P. J. Steinhardt. k-essence as a model for dark energy. *Physical Review Letters*, 85(15):4438–4441, 2001.

[22] Nandan Roy, Sangita Goswami, and Sudipta Das. Quintessence or phantom: study of scalar field dark energy models through a general parametrization of the hubble parameter. *Physics of the Dark Universe*, 36:101037, 2022.

[23] Aritra Banerjee, Haiying Cai, Lavinia Heisenberg, Eoin Ó. Colgáin, M. M. Sheikh-Jabbari, and Tao Yang. Hubble sinks in the low-redshift swampland. *Phys. Rev. D*, 103(8):L081305, 2021.

[24] Bum-Hoon Lee, Wonwoo Lee, Eoin Ó. Colgáin, M. M. Sheikh-Jabbari, and Somyadip Thakur. Is local H $_0$ at odds with dark energy EFT? *JCAP*, 04(04):004, 2022.

[25] C. Krishnan, E. Ó. Colgáin, M. M. Sheikh-Jabbari, and Tao Yang. Running Hubble Tension and a H0 Diagnostic. *Phys. Rev. D*, 103(10):103509, 2021.

[26] Nandan Roy. Exploring the possibility of interacting quintessence model as an alternative to the ΛCDM model. *Gen. Rel. Grav.*, 55(10):115, 2023.

[27] Nandan Roy and L. Arturo Ureña López. Tracker behaviour of quintom dark energy and the Hubble tension. 12 2023.

[28] A. G. Adame et al. DESI 2024 VI: Cosmological Constraints from the Measurements of Baryon Acoustic Oscillations. 4 2024.

[29] R. Calderon et al. DESI 2024: Reconstructing Dark Energy using Crossing Statistics with DESI DR1 BAO data. 5 2024.

[30] Nandan Roy, Sangita Goswami, and Sudipta Das. Quintessence or phantom: Study of scalar field dark energy models through a general parametrization of the Hubble parameter. *Phys. Dark Univ.*, 36:101037, 2022.

[31] Nandan Roy. Dynamical dark energy in the light of DESI 2024 data. 6 2024.

[32] Bikash R. Dinda. A new diagnostic for the null test of dynamical dark energy in light of DESI 2024 and other BAO data. *JCAP*, 09:062, 2024.

[33] Bikash R. Dinda and Roy Maartens. Model-agnostic assessment of dark energy after DESI DR1 BAO. 7 2024.

[34] Francisco X. Linares Cedeño, Nandan Roy, and L. Arturo Ureña López. Tracker phantom field and a cosmological constant: Dynamics of a composite

dark energy model. *Phys. Rev. D*, 104(12):123502, 2021.

[35] Anjan A. Sen, Shahnawaz A. Adil, and Somasri Sen. Do cosmological observations allow a negative Λ? *Mon. Not. Roy. Astron. Soc.*, 518(1):1098–1105, 2022.

[36] J. Alberto Vázquez, David Tamayo, Gabriela Garcia-Arroyo, Isidro Gómez-Vargas, Israel Quiros, and Anjan A. Sen. Coupled multiscalar field dark energy. *Phys. Rev. D*, 109(2):023511, 2024.

[37] Shahnawaz A. Adil, Upala Mukhopadhyay, Anjan A. Sen, and Sunny Vagnozzi. Dark energy in light of the early JWST observations: case for a negative cosmological constant? *JCAP*, 10:072, 2023.

[38] Nandan Roy and Nivedita Bhadra. Dynamical systems analysis of phantom dark energy models. *JCAP*, 1806:002, 2018.

[39] Nandan Roy, Alma X. Gonzalez-Morales, and L. Arturo Urena-Lopez. New general parametrization of quintessence fields and its observational constraints. *Phys. Rev.*, D98(6):063530, 2018.

[40] Nandan Roy and Narayan Banerjee. Tracking quintessence: a dynamical systems study. *Gen. Rel. Grav.*, 46:1651, 2014.

[41] Nandan Roy and Narayan Banerjee. Quintessence Scalar Field: A Dynamical Systems Study. *Eur. Phys. J. Plus*, 129:162, 2014.

[42] Nandan Roy and Narayan Banerjee. Dynamical systems study of Chameleon scalar field. *Annals Phys.*, 356:452–466, 2015.

[43] Nandan Roy and Narayan Banerjee. Generalized Brans-Dicke Theory: A Dynamical Systems Analysis. *Phys. Rev. D*, 95(6):064048, 2017.

[44] Zhang Cong, Zhang Han, Yuan Shuo, Liu Siqi, Zhang Tong-Jie, and Sun Yan-Chun. Four new observational h(z) data from luminous red galaxies in the sloan digital sky survey data release seven. *Research in Astronomy and Astrophysics*, 14(10):1221, oct 2014.

[45] Joan Simon, Licia Verde, and Raul Jimenez. Constraints on the redshift dependence of the dark energy potential. *Phys. Rev. D*, 71:123001, Jun 2005.

[46] M Moresco, A Cimatti, R Jimenez, L Pozzetti, G Zamorani, M Bolzonella, J Dunlop, F Lamareille, M Mignoli, H Pearce, P Rosati, D Stern, L Verde, E Zucca, C.M Carollo, T Contini, J.-P Kneib, O. Le Fè vre, S.J Lilly, V Mainieri, A Renzini, M Scodeg-gio, I Balestra, R Gobat, R McLure, S Bardelli, A Bongiorno, K Caputi, O Cucciati, S. de la Torre, L. de Ravel, P Franzetti, B Garilli, A Iovino, P Kampczyk, C Knobel, K Kovač, J.-F. Le Borgne, V. Le Brun, C Maier, R Pelló, Y Peng, E Perez-Montero, V Presotto, J.D Silverman, M Tanaka, L.A.M Tasca, L Tresse, D Vergani, O Almaini, L Barnes, R Bordoloi, E Bradshaw, A Cappi, R Chuter, M Cirasuolo, G Coppa, C Diener, S Foucaud, W Hartley, M Kamionkowski, A.M Koekemoer, C López-Sanjuan, H.J McCracken, P Nair, P Oesch, A Stanford, and N Welikala. Improved constraints on the expansion rate of the universe up to z   1.1 from the spectroscopic evolution of cosmic chronometers. *Journal of Cosmology and Astroparticle Physics*, 2012(08):006–006, aug 2012.

[47] Antonio J. Cuesta et al. The clustering of galaxies in the SDSS-III Baryon Oscillation Spectroscopic Survey: Baryon Acoustic Oscillations in the correlation function of LOWZ and CMASS galaxies in Data Release 12. *Mon. Not. Roy. Astron. Soc.*, 457(2):1770–1785, 2016.

[48] Chris Blake et al. The WiggleZ Dark Energy Survey: Joint measurements of the expansion and growth history at z < 1. *Mon. Not. Roy. Astron. Soc.*, 425:405–414, 2012.

[49] A. L. Ratsimbazafy, S. I. Loubser, S. M. Crawford, C. M. Cress, B. A. Bassett, R. C. Nichol, and P. Väisänen. Age-dating Luminous Red Galaxies observed with the Southern African Large Telescope. *Mon. Not. Roy. Astron. Soc.*, 467(3):3239–3254, 2017.

[50] Daniel Stern, Raul Jimenez, Licia Verde, Marc Kamionkowski, and S. Adam Stanford. Cosmic Chronometers: Constraining the Equation of State of Dark Energy. I: H(z) Measurements. *JCAP*, 02:008, 2010.

[51] Michele Moresco. Raising the bar: new constraints on the Hubble parameter with cosmic chronometers at z ∼ 2. *Mon. Not. Roy. Astron. Soc.*, 450(1):L16–L20, 2015.

[52] Timothée Delubac et al. Baryon acoustic oscillations in the Lyα forest of BOSS DR11 quasars. *Astron. Astrophys.*, 574:A59, 2015.

[53] Michael Blomqvist et al. Broadband distortion modeling in Lyman-α forest BAO fitting. *JCAP*, 11:034, 2015.